



Published in final edited form as:

Cell Rep. 2021 May 25; 35(8): 109162. doi:10.1016/j.celrep.2021.109162.

Non-autonomous regulation of germline stem cell proliferation by somatic MPK-1/MAPK activity in *C. elegans*

Sarah Robinson-Thiewes^{1,4}, Benjamin Dufour^{2,4}, Pier-Olivier Martel^{2,4}, Xavier Lechasseur², Amani Ange Danielle Brou², Vincent Roy^{2,3}, Yunqing Chen², Judith Kimble¹, Patrick Narbonne^{2,3,5,*}

¹Department of Genetics, University of Wisconsin-Madison, Madison, WI 53706-1580, USA

²Département de Biologie Médicale, Université du Québec à Trois-Rivières, Trois-Rivières, QC G9A 5H7, Canada

³Département de Biologie Moléculaire, de Biochimie Médicale et de pathologie, Faculté de Médecine, Université Laval, QC G1R 3S3, Canada

⁴These authors contributed equally

⁵Lead contact

SUMMARY

Extracellular-signal-regulated kinase (ERK)/mitogen-activated protein kinase (MAPK) is a major positive regulator of cell proliferation, which is often upregulated in cancer. However, few studies have addressed ERK/MAPK regulation of proliferation within a complete organism. The *Caenorhabditis elegans* ERK/MAPK ortholog MPK-1 is best known for its control of somatic organogenesis and germline differentiation, but it also stimulates germline stem cell proliferation. Here, we show that the germline-specific MPK-1B isoform promotes germline differentiation but has no apparent role in germline stem cell proliferation. By contrast, the soma-specific MPK-1A isoform promotes germline stem cell proliferation non-autonomously. Indeed, MPK-1A functions in the intestine or somatic gonad to promote germline proliferation independent of its other known roles. We propose that a non-autonomous role of ERK/MAPK in stem cell proliferation may be conserved across species and various tissue types, with major clinical implications for cancer and other diseases.

This is an open access article under the CC BY-NC-ND license (<http://creativecommons.org/licenses/by-nc-nd/4.0/>).

*Correspondence: patrick.narbonne@uqtr.ca.

AUTHOR CONTRIBUTIONS

S.R.-T. contributed Figures 1A, 1C, 1D, 2, and S3 and Tables S1 and S6, including all related strains, participated in study design, manuscript drafting, and editing; B.D. provided Figures 1E, 1F, S1, and S2; P.-O.M. constructed pPOM5-9 and provided Figures S4 and S5 and Table S3; X.L. constructed pXA2; A.A.D.B. provided Figure 1G (*fog-1, let-60 gf*); V.R. provided Figure 1G (*lin-3*); Y.C. helped with aspects of Figure S5 and Table S3; J.K. provided manuscript drafting and editing; and P.N. provided Figures 1B, 3, 4 (with help from P.-O.M. for Figures 4A–4I), and 5 (with help from V.R.) and Tables S2, S4, and S5, general study design, coordination, plasmid design, and manuscript drafting and editing. All authors approved the manuscript's final version.

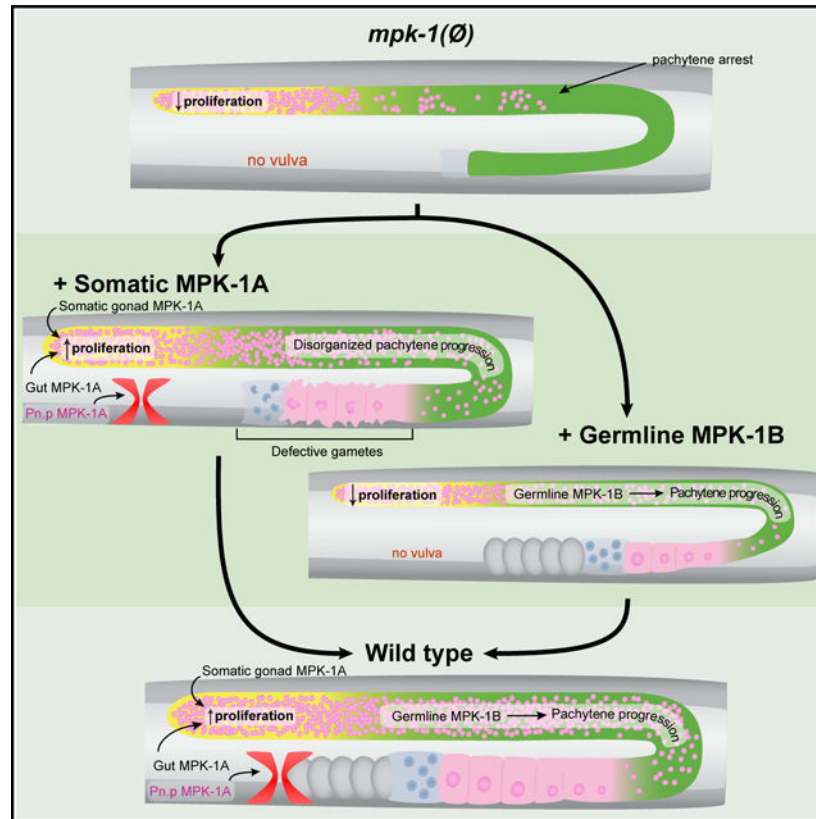
SUPPLEMENTAL INFORMATION

Supplemental information can be found online at <https://doi.org/10.1016/j.celrep.2021.109162>.

DECLARATION OF INTERESTS

The authors declare no competing interests.

Graphical Abstract



In brief

The prevailing paradigm is that ERK/MAPK functions autonomously to promote cell proliferation upon mitogen stimulation. Robinson-Thiewes et al. now demonstrate that *C. elegans* ERK/MAPK acts within somatic tissues to non-autonomously promote the proliferation of germline stem cells. Germline ERK/MAPK is thus dispensable for germline stem cell proliferation.

INTRODUCTION

The extracellular signal-regulated kinase (ERK)/mitogen-activated protein kinase (MAPK) is the downstream effector of a conserved pathway that is often upregulated in cancer (Davoli et al., 2013; Schneider et al., 2017; Shain et al., 2018). The prevailing paradigm is that activated ERK/MAPK functions cell autonomously, responding to growth factors in cells where it promotes proliferation (Meng et al., 2018; Shaul and Seger, 2007). However, the role of ERK/MAPK in stem cells (SCs) has been perplexing. Most data indicate that ERK/MAPK is dispensable for SC proliferation but required for differentiation (Burdon et al., 1999; Lu et al., 2008; Tee et al., 2014; Ying et al., 2008). Although loss of ERK1/2 in mammalian embryonic SCs reduces proliferation in culture, that effect may be secondary (Chen et al., 2015; Göke et al., 2013; Thomson et al., 1998). The effect of ERK/MAPK on SC proliferation in an organism remains largely unexplored.

We investigated how ERK/MAPK affects SC proliferation in *Caenorhabditis elegans*. The *C. elegans* genome encodes a single ortholog of mammalian ERK1/2 MAPKs, MPK-1. In *mpk-1(ø)* null mutants, several somatic organs fail to develop properly (e.g., vulva) (Sundaram, 2013; Lackner and Kim, 1998; Lackner et al., 1994), and the germline fails to progress through the meiotic cell cycle, which causes sterility (Church et al., 1995; Lee et al., 2007a, 2007b). Germline SC (GSC) proliferation is also reduced, but not arrested, in *mpk-1(ø)* mutants (Narbonne et al., 2017; Lee et al., 2007b). Therefore, as in other species and SC types, nematode ERK/MAPK is essential for differentiation but not for proliferation.

The *C. elegans* hermaphrodite gonad houses two U-shaped gonadal arms (Figure 1A, left), and germ cell maturation occurs along their distal-proximal axis (Figure 1A, right). A pool of proliferative GSCs is maintained at the distal end within a somatic niche; as GSC daughters leave the niche, they begin differentiation and progressively mature into gametes at the proximal end (Hubbard and Schedl, 2019; Lee et al., 2016; Shin et al., 2017; Haupt et al., 2019; Morrison and Kimble, 2006). GSCs, together with their proliferating progeny, span a region termed the progenitor zone (PZ) (Figure 1A, right). The GSC proliferation rate is inferred from the mitotic index (MI) across the PZ (Narbonne et al., 2015, 2017; Hubbard and Schedl, 2019, Crittenden et al., 2006). In adults, GSC proliferation affects distal-to-proximal germ cell flow and is linked to oocyte production (Nadarajan et al., 2009). Once germ cells leave the PZ, they undergo meiotic prophase and gametogenesis, making sperm in larvae and oocytes in adults.

C. elegans GSC proliferation rates are controlled jointly by ERK/MAPK (see above) and insulin/IGF-1 signaling (IIS) (Figure 1B). IIS promotes proliferation downstream of nutrient uptake (Figure 1B), a regulation conserved in worms, flies, and likely, mammals (Drummond-Barbosa and Spradling, 2001; Michaelson et al., 2010; Narbonne and Roy, 2006; Shim et al., 2013). Most relevant here, downstream IIS effectors act autonomously within the germline (Michaelson et al., 2010; Narbonne et al., 2017). In parallel, but through an unknown mechanism, MPK-1 combines with IIS to promote high proliferation typical of young adult hermaphrodites (Figure 1B) (Narbonne et al., 2017).

One aspect of the MPK-1 role in germline proliferation was clarified in studies of homeostatic regulation. GSC proliferation plummets in well-fed hermaphrodites that accumulate unfertilized oocytes because of a lack of sperm (Narbonne et al., 2015, 2017; Cinquin et al., 2016; Morgan et al., 2010). This homeostatic lowering of proliferation occurs even though IIS remains active but requires inhibition of MPK-1 signaling (Narbonne et al., 2015, 2017). The control occurs specifically in the sperm-depleted gonad arm (Narbonne et al., 2015) and, therefore, must be localized to that arm. Although molecular details may differ, homeostatic SC regulation is a common phenomenon found, for example, in fly hematopoietic and gut SCs, and in mammalian hair follicle SCs (Jiang et al., 2009; Mondal et al., 2011; Hsu et al., 2014).

An outstanding question remains how ERK/MAPK controls SC proliferation *in vivo*. The primary focus of this work is to understand how *C. elegans* MPK-1 promotes GSC proliferation. We find that MPK-1 acts in the animal's gut or somatic gonad to promote a high rate of GSC proliferation. Its action is, therefore, non-autonomous. This finding

challenges the prevailing view that ERK/MAPK controls proliferation autonomously. It, therefore, has potential to affect our understanding of ERK/MAPK control of SC proliferation during development, homeostatic regulation, and tumor formation, with implications for all organisms.

RESULTS

MPK-1 has low, but significant, kinase activity in wild-type GSCs

MPK-1 promotes a high rate of GSC proliferation in young adult hermaphrodites (Narbonne et al., 2017). Although MPK-1 protein is present in GSCs, its catalytically active form, diphosphorylated MPK-1 (dpMPK-1), has been reported only in meiotic germs cells and oocytes (Lee et al., 2007a, 2007b; Miller et al., 2001). The apparent lack of active MPK-1 in GSCs led us to ask how MPK-1 affects germline proliferation. We first used a sensitive *in vivo* ERK nuclear kinase translocation reporter (ERK-nKTR) to reassess MPK-1 activity in GSCs (de la Cova et al., 2017). This GFP-tagged sensor harbors three MPK-1-specific phosphorylation sites that control its subcellular localization. An unphosphorylated GFP reporter is retained in the nucleus but is exported to the cytoplasm when phosphorylated (Figure 1C). The ratio of cytoplasmic to nuclear GFP, thus, provides an index of MPK-1 activity. A control reporter lacking MPK-1 sites, ERK-nKTR(AAA), established the baseline ratio of cytoplasmic to nuclear GFP. Ratios above the baseline were scored as the MPK-1 activity index (see Method details).

We first assessed MPK-1 activity in wild-type (WT) adult hermaphrodites. Specifically, MPK-1 activity index was determined in PZ cells binned by distance from the distal end (Figure 1D). MPK-1 indices were higher than baseline throughout the PZ (Figures 1E and S1). Our assay also detected higher activity in pachytene and oocytes (Figure S1) (Lee et al., 2007a, 2007b; Miller et al., 2001). The sensor specifically reports MPK-1 activity as indices were below baseline in *mpk-1(∅)* germlines (Figures 1F and S1). The discovery of MPK-1 activity in GSCs, although low, raised the possibility that MPK-1 acts autonomously to promote GSC proliferation.

We used three mutants to ask whether GSC MPK-1 activity corresponds with proliferation. The *lin-3(∅)* and *fog-1(∅)* mutants have lowered rates of GSC proliferation because of homeostatic feedback: *lin-3(∅)* accumulates endomitotic oocytes, whereas *fog-1(∅)* mutants accumulate unfertilized oocytes (Figure S2) (Morgan et al., 2013; Narbonne et al., 2015; Clandinin et al., 1998). The MI was very low in both mutants (Figure 1G). PZ MPK-1 activity was undetectable in *lin-3(∅)* but similar to WT in *fog-1(∅)* (Figure 1F). Moreover, a gain-of-function (*gf*) mutant in *let-60/Ras*, expected to increase MPK-1 activity (Church et al., 1995; Lackner et al., 1994), had undetectable MPK-1 activity in the PZ (Figure 1F), although proliferation was about the same as that of WT hermaphrodites (Figure 1G). Therefore, MPK-1 activity in the PZ is not coupled to GSC proliferation. We next asked whether MPK-1 might promote proliferation from pachytene or oocyte regions. MPK-1 activity levels in pachytene and oocytes corresponded with GSC MIs (Figures 1G, S1M, and S1N), making possible a non-autonomous action from one germline region to another (although see below). Regardless, we conclude that MPK-1 activity levels in GSCs are unrelated to proliferation and unlikely to be causative.

MPK-1B autonomously promotes germline differentiation

To explore how MPK-1 promotes GSC proliferation, we assessed the expression and function of its two isoforms. The *mpk-1* locus encodes two transcripts: *mpk-1b* is longer and possesses a unique first exon, whereas *mpk-1a* shares all other exons with *mpk-1b* (Figure 2A) (Lee et al., 2007a; Lackner and Kim, 1998; Lackner et al., 1994). Previous work showed that *mpk-1b* is the main germline isoform but did not address isoform-specific expression or germline function (Lee et al., 2007a). We first inserted epitope tags into the endogenous *mpk-1* locus using CRISPR-Cas9 gene editing (Paix et al., 2015). A V5 tag inserted into the *mpk-1b*-specific exon labeled MPK-1B protein specifically, and two OLLAS tags inserted into the shared C terminus labeled both MPK-1A and MPK-1B (Figure 2A). We dub this dual-tagged locus *mpk-1(DT)*. We next created an *mpk-1b*-specific deletion, called *mpk-1b(Δ)*, and a 2,221-bp, in-frame deletion of regions common to the two isoforms, called *mpk-1(Δ)* (Figure 2A). These alleles allowed unambiguous determination of where each isoform is expressed and their respective biological roles.

We assayed MPK-1A and B expression in dissected gonads, which include the entire germline tissue plus several somatic gonadal cells, including 10 sheath cells. Some samples included extruded gut. We used α-ERK to recognize all MPK-1, with or without epitope tags (Lee et al., 2007a, 2007b), and α-V5 and α-OLLAS to recognize tagged MPK-1. WT gonads stained robustly with α-ERK, as previously reported (Lee et al., 2007a, 2007b), but not with α-V5 or α-OLLAS (Figures 2B and S3A). The *mpk-1(DT)* gonads stained robustly with all three antibodies (Figures 2C, S3B, and S3C). Intense germline staining in WT and *mpk-1(DT)* precluded visualization of staining in the somatic gonad. However, the *mpk-1(DT)* gut had strong α-ERK and α-OLLAS staining but no α-V5 (Figure S3C). We next stained *mpk-1b(Δ)* gonads, which have OLLAS-tagged MPK-1A but no MPK-1B or V5. α-ERK, α-OLLAS, and α-V5 signals were undetectable in *mpk-1b(Δ)* germlines (Figure 2D), whereas α-ERK and α-OLLAS became visible in the somatic sheath (Figure 2D, orange arrowheads). Thus, MPK-1A is the somatic isoform (expressed in the gut and somatic gonad, but not germline), whereas MPK-1B is the germline isoform (expressed in germline, but not the gut).

To learn the function of the two isoforms, we first scored fertility and vulva formation. WT and *mpk-1(DT)* animals were fertile, had a normal vulva, and were indistinguishable (Figure S3H). Thus, the tags do not affect MPK-1 function. By contrast, *mpk-1(Δ)* and *mpk-1b(Δ)* mutants were sterile, and *mpk-1(Δ)* mutants were vulvaless (Figure S3H). The *mpk-1(Δ)* defects match those of *mpk-1(Δ)* mutants (Lackner and Kim, 1998), but *mpk-1b(Δ)* do not. Together, these data indicate that germline-specific MPK-1B functions autonomously to promote fertility because its removal results in sterility and that MPK-1A promotes vulva development in *mpk-1b(Δ)* mutants.

Intriguingly, *mpk-1(Δ)* and *mpk-1b(Δ)* germlines were different. To understand those differences, we stained them with DNA, sperm, and oocyte markers. The WT germlines were large with organized germ cells in the pachytene region, a row of oocytes proximally, and sperm in the spermatheca (Figure 2E; Table S1). By contrast, *mpk-1(Δ)* germlines were smaller, had a disordered pachytene region, and failed to produce gametes (Figure 2F; Table S1), as in *mpk-1(Δ)* mutants (Lee et al., 2007a, 2007b). The *mpk-1b(Δ)* germlines had a

disorganized pachytene region, indicating a defect in pachytene progression (Figure 2G; Table S1). However, *mpk-1b*(Δ) germlines were similar in size to WT germlines. In addition, most *mpk-1b*(Δ) germlines began gamete formation, with 95% of germlines staining positive for a sperm marker and 66% also staining for an oocyte marker (Figure 2G; Table S1). However, sperm and oocytes were not arranged normally: sperm were intermingled with cells staining with the oocyte marker (Figures 2G'–2G'''). We draw two conclusions. First, MPK-1B is required for organization of the pachytene region but dispensable for pachytene exit and initiation of gametogenesis. Second, MPK-1A can initiate gametogenesis in *mpk-1b*(Δ) mutants, although gametes are aberrant. Because MPK-1A is not expressed in the germline, those effects must be non-autonomous.

We were struck that some *mpk-1b*(Δ) gonad arms seemed larger than WT gonad arms (compare Figure 2G to Figure 2E). We, therefore, calculated gonad arm volumes and counted germ nuclei in WT, *mpk-1*(Δ), and *mpk-1b*(Δ). The *mpk-1*(Δ) arms were smaller than those of WT by both volume and number of nuclei. The *mpk-1b*(Δ) gonadal arm, on the other hand, had a volume similar to a WT arm (Figure 2H), but nuclei number was reduced by ~25% (Figure 2I). Therefore, *mpk-1b*(Δ) mutants make a germline of comparable size to WT but with fewer nuclei. Because *mpk-1b*(Δ) retains activity of the MPK-1A isoform, we infer that somatic MPK-1A promotes germline growth, both in terms of volume and germ cell number.

Germline MPK-1B does not promote germline proliferation

We next tested the roles of MPK-1A and -B in GSC proliferation. Using a single-copy transgene driven by a germline-specific promoter (Dickinson et al., 2013; Frøkjær-Jensen et al., 2008), we expressed GFP::MPK-1B in *mpk-1*(\emptyset) mutants (henceforth, *germline::MPK-1B*). This strain is effectively a null mutant for MPK-1A: it has MPK-1B activity in the germline but lacks MPK-1A in the soma. MPK-1B rescued *mpk-1*(\emptyset) sterility but not its vulva defects. Animals made progeny, but without a vulva, embryos hatched inside their mother (Figures 3A–3D). The vulva defect confirms its lack of somatic MPK-1 activity. The *germline::MPK-1B* and *mpk-1b*(Δ) results are thus complementary and together show that MPK-1B is sufficient for meiotic progression and formation of gametes. MPK-1B is also necessary for formation of functional gametes. We conclude that MPK-1B acts autonomously to promote meiotic progression and gametogenesis.

The GSC MI is lower in *mpk-1*(\emptyset) mutants than it is in WT (Figure 3E) (Narbonne et al., 2017). PZ cell number is also reduced (Figure 3F). Because germline MPK-1B was sufficient to restore fertility in *mpk-1*(\emptyset), we asked whether it also restored GSC MI and PZ cell number. However, germline MPK-1B did not restore either (Figures 3E and 3F). The simple explanation was that MPK-1A acts in the soma to influence both GSC MI and PZ size. To test that idea, we scored *mpk-1b*(Δ) mutants for those two traits and found that GSC MI and PZ cell number were normal (Figures 3E and 3F). We draw three conclusions. First, somatic MPK-1A is required for normal PZ cell number. Second, germline MPK-1B does not promote high GSC proliferation rate; the reduction in total germ cell number in *mpk-1b*(Δ) germlines likely reflects problems in meiotic progression. Third and most

important, somatic MPK-1A acts non-autonomously to promote the high GSC proliferation typical of young adult hermaphrodites, whereas germline MPK-1B is dispensable.

MPK-1A promotes germline proliferation non-autonomously from the soma

To learn where MPK-1A acts in the soma to promote GSC proliferation, we turned to transgenic arrays driving GFP::MPK-1A expression in somatic tissues in an *mpk-1(∅)* mutant. Because arrays are silenced in the germline (Mello et al., 1991; Kelly and Fire, 1998), expression was limited to somatic tissues. To follow the presence of arrays, we used muscle-expressed mCherry (henceforth, *muscle::mCherry*) as a co-transformation marker, which also provided vulva muscle landmarks (Figures 4A–4I, yellow arrowheads: normal). Our negative control expressed *muscle::mCherry* alone in *mpk-1(∅)* mutants and had no rescuing effect (Figure 4B). Our positive control carried muscle-expressed mCherry plus GFP::MPK-1A expressed in all somatic cells under control of the *sur-5* promoter (henceforth, *soma::MPK-1A*) (Gu et al., 1998). The *sur-5* promoter drove strong GFP::MPK-1A expression in the gut and lower levels in all other somatic cell types (Figure 4C). The *soma::MPK-1A* rescued vulva formation, albeit not in all animals, likely because of mosaicism (Figures 5A–5C and S4; Table S2). Importantly, *soma::MPK-1A* restored the GSC MI (Figure 4J). However, *soma::MPK-1A* did not rescue fertility (Figures 4A–4C; Table S3), confirming that germline MPK-1B is essential for germline function. When *soma::MPK-1A* and *germline::MPK-1B* were combined in *mpk-1(∅)* mutants, fertility and vulva development were both rescued (Figure 4D; Table S3). Surprisingly, PZ cell counts remained lower than in controls in both *soma::MPK-1A* and *soma::MPK-1A; germline::MPK-1B* animals (Figure 4K). We do not understand why PZ size was not restored by ubiquitous somatic MPK-1A expression because it was normal in *mpk-1b()* animals (Figure 3F), which only possess somatic MPK-1A. However, we suspect that transgenic mis-expression had a role because *soma::MPK-1A* sometimes induced a multi-vulva (Table S2), a sign of MPK-1 hyperactivity (Lackner and Kim, 1998). Furthermore, the PZ size in *soma::MPK-1A; germline::MPK-1B* was significantly greater than in *soma::MPK-1A* (Figure 4K). The array transgene rescuing somatic MPK-1A may, thus, have undergone rapid stabilizing selection after the strain became fertile. We re-analyzed the PZ size of *soma::MPK-1A; germline::MPK-1B* after about a year of laboratory culture, and it was then fully restored (Figure 4K). This progressive PZ size rescue argues that it may be the result of transgenic expression being stabilized or fine-tuned over time by selective pressure. Interestingly, the GSC MI-specific rescue that occurred in *soma::MPK-1A* animals shows that GSC proliferation rates can be altered without affecting the PZ size and that the two parameters may be regulated independently by somatic MPK-1A. Regardless, we conclude that somatic MPK-1A is sufficient to drive the high GSC proliferation typical of young adult hermaphrodites and, therefore, acts non-autonomously.

We next used tissue-specific promoters to drive MPK-1A in individual somatic tissues of *mpk-1(∅)* animals. Specifically, we used *rgef-1*, *dpy-7*, *elt-7*, *myo-3*, and *ckb-3* promoters to drive expression in the nervous system, hypodermis, gut, non-pharyngeal muscles, and somatic gonad, respectively (Stefanakakis et al., 2015; Gilleard et al., 1997; Sommermann et al., 2010; Ahnn and Fire, 1994; Tenen and Greenwald, 2019). We achieved high GFP::MPK-1A expression in the nervous system and non-pharyngeal muscles, intermediate

levels in hypodermis and gut, and lower levels in somatic gonad (Figures 4E–4I). Tissue-specific expression of MPK-1A in either gut or somatic gonad fully rescued the GSC MI of *mpk-1(∅)* mutants (Figure 4J). By contrast, expression in the nervous system, non-pharyngeal muscles or hypodermis did not affect the MI (Figure 4J). As seen in *soma::MPK-1A* animals, none of the tissue-specific promoters rescued PZ size (Figure 4K). We conclude that MPK-1A acts either in the gut or in the somatic gonad to non-autonomously support the high GSC proliferation that is observed in young adult hermaphrodites.

MPK-1A promotes germline proliferation independently of other known roles

In addition to *mpk-1(∅)* defects in vulva and germline development, we noticed two additional defects. The mutants wander outside the bacterial lawn more often than WT animals do (Figure S5A), likely because of a chemotaxis defect (Hirotzu et al., 2000), and their average body length was 10% longer than in the WT (Figure S5B). We considered the idea that one of these defects might be linked to reduced GSC proliferation. If true, that defect should be rescued concurrently with GSC proliferation. We found that MPK-1A expression in either somatic gonad or muscles restored the wandering behavior, whereas gut, neuron, and hypodermis MPK-1A, or germline MPK-1B, had no effect (Figure S5A). For body length, MPK-1A expression in any somatic tissue (except for the gut) prevented excessive elongation, whereas germline MPK-1B had no effect (Figure S5B). Overall, both defects were rescued without concurrent rescue of GSC proliferation, and conversely, GSC proliferation could be rescued without concurrent rescue of the wandering or body length defects (Figures 4J, 5, and S5). We conclude that MPK-1A activity in the gut or somatic gonad promotes GSC proliferation independent of these other defects.

DISCUSSION

Before this work, evidence for MPK-1 regulation of germline proliferation was paradoxical. MPK-1 promoted GSC proliferation, as deduced from *mpk-1(∅)* mutants (Lee et al., 2007b; Narbonne et al., 2017), but active MPK-1 was not seen in proliferating germ cells, instead, being restricted to meiotic germ cells. To address that paradox, we used a highly sensitive reporter to identify low MPK-1 activity in proliferating germ cells. However, we showed that MPK-1 activity levels in proliferating germ cells did not correlate with their proliferation rate; perhaps, MPK-1 activity plays some other role within GSCs, possibly in genomic integrity (Chen et al., 2015).

The paradox was solved by identifying the individual functions of the two ERK/MAPK isoforms, one expressed in the germline and the other in the soma. We created animals that express somatic MPK-1A but not germline MPK-1B, and vice versa. Remarkably, germline proliferation was normal in MPK-1A-only animals but not in MPK-1B-only animals. Therefore, somatic MPK-1A is the key driver of germline proliferation and must act non-autonomously. However, either somatic MPK-1A or germline MPK-1B can promote more-extensive germline differentiation than seen in *mpk-1(∅)* mutants. Germline MPK-1B is sufficient to ensure formation of fully functional gametes, whereas somatic MPK-1A provides a non-autonomous boost to differentiation (Figure 5). In the absence of MPK-1B,

that MPK-1A boost is sufficient for pachytene exit and initiation of gametogenesis but gametes are not functional.

The non-autonomous effect of *C. elegans* ERK/MAPK on germline proliferation relies on expression in the gut or somatic gonad (Figure 5). Intriguingly, gap junctions interconnect gut and somatic gonad as well as somatic gonad and germ cells; moreover, those gap junctions are essential for germline proliferation (Starich et al., 2014). Although speculative, an attractive idea is that somatic MPK-1A activity uses gap junctions to stimulate germline proliferation. In mice, ERK/MAPK phosphorylation of connexins modulates gap junction opening during epidermal wound healing (Lastwika et al., 2019; Solan and Lampe, 2014). By analogy, MPK-1A could modulate gap junctions to allow unidentified proliferation-stimulatory small molecules entry into the germline. Alternatively, or in addition, MPK-1A could modulate the generation of such small molecules. Although their identity is unknown, one possibility is uridine or thymidine. That idea emerges from a study showing that cytidine deaminases (*ccd*), enzymes that make uridine and thymidine from cytidine, are required for normal germline proliferation; remarkably, the defective germline proliferation in *ccd* mutants is rescued by expression of cytidine deaminase in the gut or somatic gonad (Chi et al., 2016), solidifying the gut-gonad-germline axis of proliferation control. However, a direct relationship between MPK-1A activity and germline uridine/thymidine levels remains highly speculative.

Discovery of a non-autonomous role for ERK/MAPK in germline proliferation has implications for the homeostatic regulation of germline proliferation. That regulation requires MPK-1 inhibition locally within the affected gonadal arm, which has both somatic and germ cells. We suggest that homeostatic inhibition of MPK-1 may occur in the gut or somatic gonad, given that MPK-1A functions there to promote proliferation (this work). We favor the somatic gonad as the likely site for MPK-1 inhibition during homeostasis because each gonadal arm is embraced independently by somatic sheath cells. By contrast, the gut runs the length of the body cavity and neighbors both gonadal arms. Because homeostatic control of proliferation occurs broadly in the animal kingdom and because regulators of SC proliferation and homeostasis are highly conserved (ERK/MAPK and IIS, see Introduction), these regulators may similarly orchestrate proliferation rates in diverse SC populations. Consistent with that, GSC proliferation in *Drosophila* is stimulated by nutrient uptake via IIS signaling (LaFever and Drummond-Barbosa, 2005), whereas homeostatic regulation of intestinal SCs occurs through ERK/MAPK regulation (Zhang et al., 2019).

The non-autonomous action of ERK/MAPK in the regulation of germline proliferation has major implications for understanding, and perhaps treating, cancer. ERK/MAPK is upregulated in many human cancers (Burotto et al., 2014; Davoli et al., 2013; Schneider et al., 2017; Shain et al., 2018), although its primary role in embryonic SCs is differentiation (Burdon et al., 1999; Lu et al., 2008; Tee et al., 2014; Ying et al., 2008). Importantly, tumors are heterogeneous, and only cancer SCs generate a new tumor upon transplantation (Tan et al., 2006; Scott et al., 2019). The bulk of the tumor, therefore, likely consists of the progeny of cancer SCs, which are in various states of differentiation. Cancer SCs are thought to develop from non-cancerous SCs as a result of replication errors (Tomasetti and Vogelstein, 2015) and thus retain the SC character. As such, cancer SCs may depend on ERK/MAPK

activity in neighboring tissues or cells to promote their proliferation—similar to *C. elegans* somatic MPK-1A ensuring high GSC proliferation. If that is the case, chemotherapy that lowers ERK/MAPK activity might either promote quiescence in cancer SCs non-autonomously and/or suppress tumor growth by autonomously inhibiting the differentiated progeny of cancer SCs.

STAR★METHODS

RESOURCE AVAILABILITY

Lead contact—Further information and requests for resources and reagents should be directed to and will be fulfilled by the lead contact, Patrick Narbonne (patrick.narbonne@uqtr.ca).

Materials availability—Key strains generated for this study will be made available through the *Caenorhabditis* Genetics Center (CGC).

Data and code availability—This study did not generate large datasets or codes, but raw data/images are available from the lead contact upon request.

EXPERIMENTAL MODEL AND SUBJECT DETAILS

***C. elegans* genetics**—Animals were maintained on standard NGM plates seeded with *E. coli* (OP50) and the Bristol isolate (N2) was used as WT throughout (Brenner, 1974). Only hermaphrodites were scored, as young adults, and with the following specifics. For Figures 1, 3, 4, S1, and S2, animals were maintained at 15°C, synchronized by picking late L4 stage larvae to a new plate (Seydoux et al., 1993), and upshifted to 25°C for 24 hours (unless otherwise specified) before they were harvested for assaying. For Figures 3 and S3, animals were maintained at 20°C and were analyzed at L4 + 24 hours. For Figures S4 and S5, animals were raised at 25°C from the L1 stage. All strains, alleles, transgenes and rearrangements used are listed in Table S4.

METHOD DETAILS

Plasmids, transgenics and genome editing—We used the Gibson et al. (2009) method for all plasmid assembly, except for pUMP5, which was generated by T/A cloning of an RT-PCR product into pMR377, a modified pKSII-based vector, after opening it with *XcmI* to generate T-overhangs (a kind gift from Shaolin Li). The source DNA and primers that were used to generate all plasmids, as well as their microinjection concentrations, are found in Table S5. Extra-chromosomal arrays were generated by regular microinjections at a total concentration of 150–200 µg/mL, using pKSII as a filler DNA and pCFJ104[*Pmyo-3::mCherry*] (5 µg/mL) as a co-injection marker (Mello et al., 1991, Frøkjær-Jensen et al., 2008). For the lines harboring pPOM5–9 altogether, each plasmid was injected at 15 µg/mL, in a single mix.

For single-copy insertion (*i.e.*, *narSi2*), pNAR3 was co-injected with pDD122 in *unc-119(ed3)* animals for CRISPR/Cas9-mediated integration at ttTi5605 on LG II (+0.77) (Dickinson et al., 2013). A single line was obtained from > 200 microinjections.

For editing the *mpk-1* locus, CRISPR/Cas9 was used according to previously described methods (Dokshin et al., 2018; Paix et al., 2014). Repair templates and crRNAs are listed in Table S6. To create the *mpk-1(DT)*, an intermediate V5-tagged strain was first generated. The 2xOLLAS tag was subsequently inserted into the V5-tagged strain to create *mpk-1(DT)*. The *mpk-1(DT)* strain was used as the starting point to generate *mpk-1b()*, but the V5-tagged strain was used to generate *mpk-1()*. All CRISPR created *mpk-1* strains were outcrossed to N2 two times. The *mpk-1b()* and *mpk-1()* alleles were maintained over the *qC1[qIs26]* balancer. Full genotypes are listed in Table S4.

Quantification of germline MPK-1 activity—Following bleach synchronization, all worms were grown at 25°C until L4 + 24 hours (A1). Animals were collected and paralyzed in 4.15 mM (0.1%) Tetramisole in M9 buffer on a coverslip that was flipped onto a 3% agarose pad and sealed using VALAP (1:1:1 Vaseline, lanolin and paraffin). A Leica confocal microscope TCS SP8 (Leica Microsystems) with a HC PL APO CS2 40x/1.30 numerical aperture oil objective was used for image collection. Bidirectional scanning at 400 Hz, in sequential mode, combined with a 0.8 μm Z stack step was used to image each gonad. Only the anterior gonad arm of each worm was acquired. ERK-nKTR::GFP was acquired using a 488 nm solid-state laser at 10% intensity, for all strains, except *fog-1(∅)*, which was at 15% intensity. PMT gate was set at 673 gain and at 559.5 ± 21.5 nm for all strains. H2B::mCherry was acquired using a 552 nm solid-state laser at 5% intensity using a HyD gate at 50% gain and at 610 ± 21 nm.

Image processing and data analysis were done with Fiji. For the PZ, cells were grouped based on distance from the distal tip (1–5, 6–10, 11–15, and 1–15). Five cells were analyzed per gonad, distributed one per three cell diameter regions. For the pachytene region, five cells per gonad were randomly chosen, but evenly distributed across the region. For oocytes, five cells per gonad were analyzed starting from the –2 oocyte to avoid sperm-activated oocytes. Variability in the H2B::mCherry intensities between germ cells and across germline regions (see Figure S1) prevented us from using the previously published quantification method, developed for vulva precursor cells (de la Cova et al., 2017). Thus, for all germ cells, the mean GFP fluorescence signal intensity was measured for three randomly-chosen circular cytoplasmic areas (0.5 μm for GSCs and pachytene; 4 μm for oocytes) and for the whole nucleus. Cell selection and cytoplasmic area selections were made using the mCherry channel to avoid introducing any user-bias after seeing the GFP channel. The three cytoplasmic GFP mean intensity measures were averaged and divided by the single mean nuclear intensity measurement to obtain an MPK-1 activity index for each cell. Five cells of each types were averaged for all strains. For each genotype, the ERK-nKTR activity index for each region was first normalized to its ERK-nKTR(AAA) control, then to the WT ERK-nKTR(AAA) control for comparison across different genotypes. As germline autofluorescence accounted for less than 1% of the GFP signal for all samples, background subtractions were omitted.

Progenitor zone and mitotic index evaluation—PZ size and MIs of young adult (L4 + 24 hours at 25°C) hermaphrodites were evaluated as previously described (Narbonne et al., 2015, 2017). Briefly, animals were picked and quickly dissected on a coverslip in a drop of

PBS, the coverslip was flipped onto a poly-L-lysine coated slide, submitted to a standard -80°C freeze-crack procedure, fixed with -20°C methanol for 1 minute, then post-fixed with 3.7% paraformaldehyde for 30 minutes. Gonads were then washed (2×10 minutes) with PBST (1xPBS + 0.1% Tween 20) and blocked in PBST+3% BSA, incubated overnight at 4°C with primary mouse anti-p[Ser10]H3 (1:250) and rabbit anti-HIM-3 (1:500) antibodies, diluted in PBST+1% BSA. Gonads were then washed (3×10 minutes) with PBST and incubated with secondary A488-coupled goat anti-mouse and A546-coupled goat anti-rabbit antibodies (1:500 each) for 1 hour at room temperature (RT). Finally, slides were washed 3 more times with PBST, briefly stained with DAPI between washes 2 and 3, before Vectashield was added and the coverslip was sealed with nail polish. Slides were kept at -20°C until analyzed. For every genotype for which we had previously published an A1 MI result (N2, *fog-1*(\emptyset), and *mpk-1*(\emptyset)) (Narbonne et al., 2015, 2017), we did not detect a significant difference between the newer and older datasets ($p > 0.05$; Kruskal-Wallis).

Immunostaining and fluorescence

Sperm/oocyte staining: Briefly, worms raised at 20°C were picked as mid-L4s to a fresh plate, 24 hours prior to staining. Hermaphrodites were anesthetized in $0.25 \mu\text{M}$ levamisole in PBST. Gonads were collected and fixed in 3.7% formaldehyde in PBST for 15 minutes while rocking at RT. After washing in 1 mL PBST, gonads were permeabilized in PBST +0.1% Triton-X and incubated for 10 minutes, rocking at RT. Gonads were washed 3×10 minutes in PBST and blocked in PBST+0.5% BSA (block) for 1 hour. After the block was removed, samples were incubated overnight at 4°C with primary antibodies diluted in the block solution, 1:200 sperm marker mouse α -sp56 and 1: 500 oocyte marker rabbit α -RME-2. Primary antibodies were removed and gonads were washed 3×10 minutes in PBST. 100 μL of block containing DAPI (1 $\mu\text{g}/\text{mL}$), α -mouse alexa647 and α -rabbit alexa555 secondary antibody (1:1000 each) was added and gonads incubated in the dark, rotating for 2 hours at RT. Gonads were washed 3×10 minutes in PBST in the dark at RT. Gonads were mounted in 18 mL Prolong Glass antifade (ThermoFisher, P36984) and sealed with VALAP. Samples were kept at -20°C until imaged.

MPK-1 staining: Hermaphrodites were staged, anesthetized and dissected as described for sperm/oocyte staining. Gonads were fixed in 2% paraformaldehyde (PFA) in 100 nM pH 7.2 K_2PO_4 for 30 minutes, rocking at RT. Gonads were washed 2x in PBST: first wash quick and second wash for 5 minutes at RT. Gonads were fixed in methanol for 30 minutes at -20°C . Gonads were washed 2x, following the same procedure as after the PFA fix. Gonads were blocked for 1 hour, rocking at RT. Primary antibodies—mouse α -V5 (Bio-Rad), rat α -OLLAS (Novis, NBP1-06713), rabbit α -ERK (Santa Cruz Biotechnology, Sc94)—were diluted 1:1000, 1:200, 1:1000 in blocking solution, respectively. Gonads incubated with primary antibodies overnight at 4°C . Gonads were then washed 2x PBST quickly and 2x PBST for 10 minutes. Secondary α -mouse alexa555, α -rat alexa647, and α -rabbit alexa488 antibodies, and DAPI (1 $\mu\text{g}/\text{mL}$) were all diluted 1:1000 in block solution and incubated for 2 hours, rocking in the dark at RT. Secondary antibodies were removed and gonads were washed 4x in PBST—2x quickly and 2x for 10 minutes in the dark. Gonads were mounted in 18 μL Prolong Glass antifade, sealed with VALAP, and stored at -20°C until imaged.

DAPI staining: Staged L4+24 hr hermaphrodites were dissected in PBST+0.25 μ M levamisole. Gonads were collected and fixed in 2% pFA for 10 minutes, rocking at RT. The fixation solution was removed; samples were washed once with PBST. The gonads were permeabilized in PBST+0.5% BSA+0.1% Triton-X for 10 minutes, rocking at RT. The permeabilization solution was removed and gonads were incubated with DAPI (1 μ g/mL) in PBST for 30 minutes, rocking in the dark at RT. Gonads were washed 3x in PBST for 10 minutes in the dark at RT. After the washes, gonads were mounted in 10 μ L Vectashield (Vector laboratories) and sealed with VALAP. Samples were kept at 4°C until imaged.

Image acquisition—For Figures 2 and S3, all images were taken using a Leica SP8 confocal microscope using a 40x oil objective (NA 1.3) with 1.5 zoom and 0.30 mm z-step. For fluorescence quantification (Figures S3E–S3G), images of the distal gonad were taken first (PZ through midpachytene region). Fluorophores alexa 488, alexa 555, alexa 647, and DAPI were excited at 488 nm, 561 nm, 633 nm, and 105 nm respectively; emissions were collected at 510–540 nm, 562–600 nm, 650–700 nm, and 425–490 nm, respectively.

The mosaic merge function of the Leica Lightening software package was used to generate Figures 2 images. For all tile scanned germlines, a custom region of interest was drawn around the tissue; images were taken using a 1024 \times 1024 window. All tiles covering the entire germline tissue were merged into one image during acquisition using default settings. We did not quantify fluorescence of the mosaic merged images because the fluorescence intensity was smoothed at tile junction points.

For Figures 3 and 4, differential interference contrast (DIC) and epifluorescence images were acquired every micron using a Plan-Apochromat 20x dry objective (NA 0.8) mounted on an inverted Zeiss Axio Observer.Z1. Images were stitched and deconvolved using the Zen software, and animals were straightened using ImageJ. Epifluorescence signals were overlaid to the DIC images using Photoshop CS6.

Gonad volume and germ cell quantification—DAPI stained mosaic-merged gonads were imported into Imaris (version 9.3.1) using the software's file converter version 9.5. Using the surfaces function, outlines of the gonads were manually drawn around every other z plane throughout the stack. Afterward, the "create surface" tool made a volume representation based on the manually drawn outlines. Then the volume was calculated in the detailed statistics tab in the surfaces menu.

The same images were used to calculate both gonad volume and germ cell numbers. Using the multipoint tool in FIJI, germ cells were manually counted from the distal end to the loop.

MPK-1 protein quantification—Fluorescence intensity was measured in FIJI using previously described methods (Crittenden et al., 2019; Haupt et al., 2019). OLLAS and V5 intensities were normalized to the N2 background. ERK intensity was normalized to the *mpk-1b* background because *mpk-1b* was previously shown to be the main germline isoform (Lee et al., 2007a). Intensity plots were generated by importing FIJI data into MATLAB using the shadedErrorBar function (Rob Campbell, <https://www.GitHub.com>, 2020).

***E. coli* attraction**—Animals were raised at 25°C until the late L4 stage and picked, in cohorts of 20–30 individuals, to the center of a 6mm NGM dish, pre-seeded with a 40 uL drop of *E. coli* (OP50) overnight culture. Plates were imaged every half-hour during hours 22–24 post-L4 (until A1). The percentage of worms on food were counted at each time point and averaged over all time points for each plate. This assay was repeated at least 4 times for each genotype.

Body length measurements—Animals were raised at 25°C until they reached A1, paralysed with tetrazimole in M9 buffer, and mounted on a 3% agarose pad. Whole animals were acquired using a 10X objective and measured using ImageJ.

QUANTIFICATION AND STATISTICAL ANALYSIS

For parametric datasets, the one-way ANOVA was used, and followed by Tukey multiple comparisons. For non-parametric datasets, the Kruskal-Wallis test was used, and followed by Dunn multiple comparisons, adjusted according to the family-wide error rate procedure of Holm, and then by the false discovery rate procedure of Benjamini-Hochberg. Statistical details of experiments can be found in the figure legends.

Supplementary Material

Refer to Web version on PubMed Central for supplementary material.

ACKNOWLEDGMENTS

We thank Shaolin Li for reagents and precious advice; Claire de la Cova, Iva Greenwald, and Alex Hajnal for strains; and WormBase for its essential role in *C. elegans* research. The Narbonne laboratory is funded by grants from the Fondation UQTR, FRQ-NT (2018-NC-205752), FRQ-S (265445), NSERC (RGPIN-2019-06863, RGPAS-2019-00017, and DGEGR-2019-00326), CIHR (PJT-169138), and CFI (36916) to P.N. P.N. is a Junior 1 Bursary Scholar (252405) of FRQ-S and holds a UQTR research chair. S.R.-T. was supported by an NSF graduate fellowship (DGE-1256259) and an NIH predoctoral training grant in genetics (5T32GM007133). J.K. was an HHMI Investigator and is now supported by NIH R01 GM134119. Some strains were provided by the CGC, which is funded by NIH Office of Research Infrastructure Programs (P40 OD010440).

REFERENCES

- Ahn J, and Fire A (1994). A screen for genetic loci required for body-wall muscle development during embryogenesis in *Caenorhabditis elegans*. *Genetics* 137, 483–498. [PubMed: 8070659]
- Brenner S (1974). The genetics of *Caenorhabditis elegans*. *Genetics* 77, 71–94. [PubMed: 4366476]
- Burdon T, Stracey C, Chambers I, Nichols J, and Smith A (1999). Suppression of SHP-2 and ERK signalling promotes self-renewal of mouse embryonic stem cells. *Dev. Biol* 210, 30–43. [PubMed: 10364425]
- Burotto M, Chiou VL, Lee JM, and Kohn EC (2014). The MAPK pathway across different malignancies: a new perspective. *Cancer* 120, 3446–3456. [PubMed: 24948110]
- Chen H, Guo R, Zhang Q, Guo H, Yang M, Wu Z, Gao S, Liu L, and Chen L (2015). Erk signaling is indispensable for genomic stability and self-renewal of mouse embryonic stem cells. *Proc. Natl. Acad. Sci. USA* 112, E5936–E5943. [PubMed: 26483458]
- Chi C, Ronai D, Than MT, Walker CJ, Sewell AK, and Han M (2016). Nucleotide levels regulate germline proliferation through modulating GLP-1/Notch signaling in *C. elegans*. *Genes Dev.* 30, 307–320. [PubMed: 26833730]

- Church DL, Guan KL, and Lambie EJ (1995). Three genes of the MAP kinase cascade, *mek-2*, *mpk-1/sur-1* and *let-60* ras, are required for meiotic cell cycle progression in *Caenorhabditis elegans*. *Development* 121, 2525–2535. [PubMed: 7671816]
- Cinquin A, Chiang M, Paz A, Hallman S, Yuan O, Vysniauskaite I, Fowlkes CC, and Cinquin O (2016). Intermittent stem cell cycling balances self-renewal and senescence of the *C. elegans* germ line. *PLoS Genet.* 12, e1005985. [PubMed: 27077385]
- Clandinin TR, DeModena JA, and Sternberg PW (1998). Inositol trisphosphate mediates a RAS-independent response to LET-23 receptor tyrosine kinase activation in *C. elegans*. *Cell* 92, 523–533. [PubMed: 9491893]
- Crittenden SL, Leonhard KA, Byrd DT, and Kimble J (2006). Cellular analyses of the mitotic region in the *Caenorhabditis elegans* adult germ line. *Mol. Biol. Cell* 17, 3051–3061. [PubMed: 16672375]
- Crittenden SL, Lee C, Mohanty I, Battula S, Knobel K, and Kimble J (2019). Sexual dimorphism of niche architecture and regulation of the *Caenorhabditis elegans* germline stem cell pool. *Mol. Biol. Cell* 30, 1757–1769. [PubMed: 31067147]
- Davoli T, Xu AW, Mengwasser KE, Sack LM, Yoon JC, Park PJ, and Elledge SJ (2013). Cumulative haploinsufficiency and triplosensitivity drive aneuploidy patterns and shape the cancer genome. *Cell* 155, 948–962. [PubMed: 24183448]
- de la Cova C, Townley R, Regot S, and Greenwald I (2017). A real-time biosensor for ERK activity reveals signaling dynamics during *C. elegans* cell fate specification. *Dev. Cell* 42, 542–553.e4. [PubMed: 28826819]
- Dernburg AF, Zalevsky J, Colaiácovo MP, and Villeneuve AM (2000). Transgene-mediated cosuppression in the *C. elegans* germ line. *Genes Dev.* 14, 1578–1583. [PubMed: 10887151]
- Dickinson DJ, Ward JD, Reiner DJ, and Goldstein B (2013). Engineering the *Caenorhabditis elegans* genome using Cas9-triggered homologous recombination. *Nat. Methods* 10, 1028–1034. [PubMed: 23995389]
- Dokshin GA, Ghanta KS, Piscopo KM, and Mello CC (2018). Robust genome editing with short single-stranded and long, partially single-stranded DNA donors in *Caenorhabditis elegans*. *Genetics* 210, 781–787. [PubMed: 30213854]
- Drummond-Barbosa D, and Spradling AC (2001). Stem cells and their progeny respond to nutritional changes during *Drosophila* oogenesis. *Dev. Biol* 231, 265–278. [PubMed: 11180967]
- Frøkjær-Jensen C, Davis MW, Hopkins CE, Newman BJ, Thummel JM, Olesen SP, Grunnet M, and Jørgensen EM (2008). Single-copy insertion of transgenes in *Caenorhabditis elegans*. *Nat. Genet* 40, 1375–1383. [PubMed: 18953339]
- Gibson DG, Young L, Chuang RY, Venter JC, Hutchison CA 111, and Smith HO (2009). Enzymatic assembly of DNA molecules up to several hundred kilobases. *Nat. Methods* 6, 343–345. [PubMed: 19363495]
- Gilleard JS, Barry JD, and Johnstone IL (1997). *cis* regulatory requirements for hypodermal cell-specific expression of the *Caenorhabditis elegans* cuticle collagen gene *dpy-7*. *Mol. Cell. Biol* 17, 2301–2311. [PubMed: 9121480]
- Göke J, Chan YS, Yan J, Vingron M, and Ng HH (2013). Genome-wide kinase-chromatin interactions reveal the regulatory network of ERK signaling in human embryonic stem cells. *Mol. Cell* 50, 844–855. [PubMed: 23727019]
- Gu T, Orita S, and Han M (1998). *Caenorhabditis elegans* SUR-5, a novel but conserved protein, negatively regulates LET-60 Ras activity during vulval induction. *Mol. Cell. Biol* 18, 4556–4564. [PubMed: 9671465]
- Haupt KA, Enright AL, Ferdous AS, Kershner AM, Shin H, Wickens M, and Kimble J (2019). The molecular basis of LST-1 self-renewal activity and its control of stem cell pool size. *Development* 146, dev181644. [PubMed: 31515205]
- Hirotsu T, Saeki S, Yamamoto M, and Iino Y (2000). The Ras-MAPK pathway is important for olfaction in *Caenorhabditis elegans*. *Nature* 404, 289–293. [PubMed: 10749212]
- Hsu YC, Li L, and Fuchs E (2014). Transit-amplifying cells orchestrate stem cell activity and tissue regeneration. *Cell* 157, 935–949. [PubMed: 24813615]
- Hubbard EJA, and Schedl T (2019). Biology of the *Caenorhabditis elegans* germline stem cell system. *Genetics* 213, 1145–1188. [PubMed: 31796552]

- Jiang H, Patel PH, Kohlmaier A, Grenley MO, McEwen DG, and Edgar BA (2009). Cytokine/Jak/Stat signaling mediates regeneration and homeostasis in the *Drosophila* midgut. *Cell* 137, 1343–1355. [PubMed: 19563763]
- Kelly WG, and Fire A (1998). Chromatin silencing and the maintenance of a functional germline in *Caenorhabditis elegans*. *Development* 125, 2451–2456. [PubMed: 9609828]
- Lackner MR, and Kim SK (1998). Genetic analysis of the *Caenorhabditis elegans* MAP kinase gene *mpk-1*. *Genetics* 150, 103–117. [PubMed: 9725833]
- Lackner MR, Kornfeld K, Miller LM, Horvitz HR, and Kim SK (1994). A MAP kinase homolog, *mpk-1*, is involved in ras-mediated induction of vulval cell fates in *Caenorhabditis elegans*. *Genes Dev.* 8, 160–173. [PubMed: 8299936]
- LaFever L, and Drummond-Barbosa D (2005). Direct control of germline stem cell division and cyst growth by neural insulin in *Drosophila*. *Science* 309, 1071–1073. [PubMed: 16099985]
- Lastwika KJ, Dunn CA, Solan JL, and Lampe PD (2019). Phosphorylation of connexin 43 at MAPK, PKC or CK1 sites each distinctly alter the kinetics of epidermal wound repair. *J. Cell Sci* 132, jcs234633. [PubMed: 31427427]
- Lee MH, Hook B, Pan G, Kershner AM, Merritt C, Seydoux G, Thomson JA, Wickens M, and Kimble J (2007a). Conserved regulation of MAP kinase expression by PUF RNA-binding proteins. *PLoS Genet.* 3, e233. [PubMed: 18166083]
- Lee MH, Ohmachi M, Arur S, Nayak S, Francis R, Church D, Lambie E, and Schedl T (2007b). Multiple functions and dynamic activation of MPK-1 extracellular signal-regulated kinase signaling in *Caenorhabditis elegans* germline development. *Genetics* 177, 2039–2062. [PubMed: 18073423]
- Lee C, Sorensen EB, Lynch TR, and Kimble J (2016). *C. elegans* GLP-1/Notch activates transcription in a probability gradient across the germline stem cell pool. *eLife* 5, e18370. [PubMed: 27705743]
- Lu CW, Yabuuchi A, Chen L, Viswanathan S, Kim K, and Daley GQ (2008). Ras-MAPK signaling promotes trophoblast formation from embryonic stem cells and mouse embryos. *Nat. Genet* 40, 921–926. [PubMed: 18536715]
- Mello CC, Kramer JM, Stinchcomb D, and Ambros V (1991). Efficient gene transfer in *C. elegans*: extrachromosomal maintenance and integration of transforming sequences. *EMBO J.* 10, 3959–3970. [PubMed: 1935914]
- Meng D, Frank AR, and Jewell JL (2018). mTOR signaling in stem and progenitor cells. *Development* 145, dev152595. [PubMed: 29311260]
- Michaelson D, Korta DZ, Capua Y, and Hubbard EJ (2010). Insulin signaling promotes germline proliferation in *C. elegans*. *Development* 137, 671–680. [PubMed: 20110332]
- Miller MA, Nguyen VQ, Lee MH, Kosinski M, Schedl T, Caprioli RM, and Greenstein D (2001). A sperm cytoskeletal protein that signals oocyte meiotic maturation and ovulation. *Science* 291, 2144–2147. [PubMed: 11251118]
- Mondal BC, Mukherjee T, Mandal L, Evans CJ, Sinenko SA, Martinez-Agosto JA, and Banerjee U (2011). Interaction between differentiating cell- and niche-derived signals in hematopoietic progenitor maintenance. *Cell* 147, 1589–1600. [PubMed: 22196733]
- Morgan DE, Crittenden SL, and Kimble J (2010). The *C. elegans* adult male germline: stem cells and sexual dimorphism. *Dev. Biol* 346, 204–214. [PubMed: 20659446]
- Morgan CT, Noble D, and Kimble J (2013). Mitosis-meiosis and spermoocyte fate decisions are separable regulatory events. *Proc. Natl. Acad. Sci. USA* 110, 3411–3416. [PubMed: 23401507]
- Morrison SJ, and Kimble J (2006). Asymmetric and symmetric stem-cell divisions in development and cancer. *Nature* 441, 1068–1074. [PubMed: 16810241]
- Nadarajan S, Govindan JA, McGovern M, Hubbard EJ, and Greenstein D (2009). MSP and GLP-1/Notch signaling coordinately regulate actomyosin-dependent cytoplasmic streaming and oocyte growth in *C. elegans*. *Development* 136, 2223–2234. [PubMed: 19502484]
- Narbonne P, and Roy R (2006). Regulation of germline stem cell proliferation downstream of nutrient sensing. *Cell Div.* 1, 29. [PubMed: 17150096]
- Narbonne P, Maddox PS, and Labbé JC (2015). DAF-18/PTEN locally antagonizes insulin signalling to couple germline stem cell proliferation to oocyte needs in *C. elegans*. *Development* 142, 4230–4241. [PubMed: 26552888]

- Narbonne P, Maddox PS, and Labbé JC (2017). DAF-18/PTEN signals through AAK-1/AMPK to inhibit MPK-1/MAPK in feedback control of germline stem cell proliferation. *PLoS Genet.* 13, e1006738. [PubMed: 28410423]
- Paix A, Wang Y, Smith HE, Lee CY, Calidas D, Lu T, Smith J, Schmidt H, Krause MW, and Seydoux G (2014). Scalable and versatile genome editing using linear DNAs with microhomology to Cas9 Sites in *Caenorhabditis elegans*. *Genetics* 198, 1347–1356. [PubMed: 25249454]
- Paix A, Folkmann A, Rasoloson D, and Seydoux G (2015). High efficiency, homology-directed genome editing in *Caenorhabditis elegans* using CRISPR-Cas9 ribonucleoprotein complexes. *Genetics* 201, 47–54. [PubMed: 26187122]
- Schneider G, Schmidt-Supprian M, Rad R, and Saur D (2017). Tissue-specific tumorigenesis: context matters. *Nat. Rev. Cancer* 17, 239–253. [PubMed: 28256574]
- Scott JG, Dhawan A, Hjelmeland A, Lathia J, Chumakova A, Hitomi M, Fletcher AG, Maini PK, and Anderson ARA (2019). Recasting the cancer stem cell hypothesis: unification using a continuum model of microenvironmental forces. *Curr. Stem Cell Rep* 5, 22–30.
- Seydoux G, Savage C, and Greenwald I (1993). Isolation and characterization of mutations causing abnormal eversion of the vulva in *Caenorhabditis elegans*. *Dev. Biol* 157, 423–436. [PubMed: 8500652]
- Shain AH, Joseph NM, Yu R, Benhamida J, Liu S, Prow T, Ruben B, North J, Pincus L, Yeh I, et al. (2018). Genomic and transcriptomic analysis reveals incremental disruption of key signaling pathways during melanoma evolution. *Cancer Cell* 34, 45–55.e4. [PubMed: 29990500]
- Shaul YD, and Seger R (2007). The MEK/ERK cascade: from signaling specificity to diverse functions. *Biochim. Biophys. Acta* 1773, 1213–1226. [PubMed: 17112607]
- Shim J, Gururaja-Rao S, and Banerjee U (2013). Nutritional regulation of stem and progenitor cells in *Drosophila*. *Development* 140, 4647–4656. [PubMed: 24255094]
- Shin H, Haupt KA, Kershner AM, Kroll-Conner P, Wickens M, and Kimble J (2017). SYGL-1 and LST-1 link niche signaling to PUF RNA repression for stem cell maintenance in *Caenorhabditis elegans*. *PLoS Genet.* 13, e1007121. [PubMed: 29232700]
- Solan JL, and Lampe PD (2014). Specific Cx43 phosphorylation events regulate gap junction turnover in vivo. *FEBS Lett.* 588, 1423–1429. [PubMed: 24508467]
- Sommermann EM, Strohmaier KR, Maduro MF, and Rothman JH (2010). Endoderm development in *Caenorhabditis elegans*: the synergistic action of ELT-2 and -7 mediates the specification/differentiation transition. *Dev. Biol* 347, 154–166. [PubMed: 20807527]
- Starich TA, Hall DH, and Greenstein D (2014). Two classes of gap junction channels mediate somat-germline interactions essential for germline proliferation and gametogenesis in *Caenorhabditis elegans*. *Genetics* 198, 1127–1153. [PubMed: 25195067]
- Stefanakis N, Carrera I, and Hobert O (2015). Regulatory logic of panneuronal gene expression in *C. elegans*. *Neuron* 87, 733–750. [PubMed: 26291158]
- Sundaram MV (2013). Canonical RTK-Ras-ERK signaling and related alternative pathways. *WormBook*, 1–38.
- Tan BT, Park CY, Ailles LE, and Weissman IL (2006). The cancer stem cell hypothesis: a work in progress. *Lab. Invest* 86, 1203–1207. [PubMed: 17075578]
- Tee WW, Shen SS, Oksuz O, Narendra V, and Reinberg D (2014). Erk1/2 activity promotes chromatin features and RNAPII phosphorylation at developmental promoters in mouse ESCs. *Cell* 156, 678–690. [PubMed: 24529373]
- Tenen CC, and Greenwald I (2019). Cell non-autonomous function of daf-18/PTEN in the somatic gonad coordinates somatic gonad and germline development in *C. elegans* dauer larvae. *Curr. Biol* 29, 1064–1072.e8. [PubMed: 30827916]
- Thomson JA, Itskovitz-Eldor J, Shapiro SS, Waknitz MA, Swiergiel JJ, Marshall VS, and Jones JM (1998). Embryonic stem cell lines derived from human blastocysts. *Science* 282, 1145–1147. [PubMed: 9804556]
- Tomasetti C, and Vogelstein B (2015). Cancer etiology; variation in cancer risk among tissues can be explained by the number of stem cell divisions. *Science* 347, 78–81. [PubMed: 25554788]
- Ying QL, Wray J, Nichols J, Battle-Morera L, Doble B, Woodgett J, Cohen P, and Smith A (2008). The ground state of embryonic stem cell self-renewal. *Nature* 453, 519–523. [PubMed: 18497825]

Zhang P, Holowatyj AN, Roy T, Pronovost SM, Marchetti M, Liu H, Ulrich CM, and Edgar BA (2019). An SH3PX1-dependent endocytosis-autophagy network restrains intestinal stem cell proliferation by counteracting EGFR-ERK signaling. *Dev. Cell* 49, 574–589.e5. [PubMed: 31006650]

Author Manuscript

Author Manuscript

Author Manuscript

Author Manuscript

Highlights

- Germline MPK-1B is dispensable for proliferation of germline stem cells
- Germline MPK-1B is essential for gametogenesis and fertility
- Somatic MPK-1A is required for a high rate of GSC proliferation
- Somatic MPK-1A promotes germline proliferation from the gut or somatic gonad

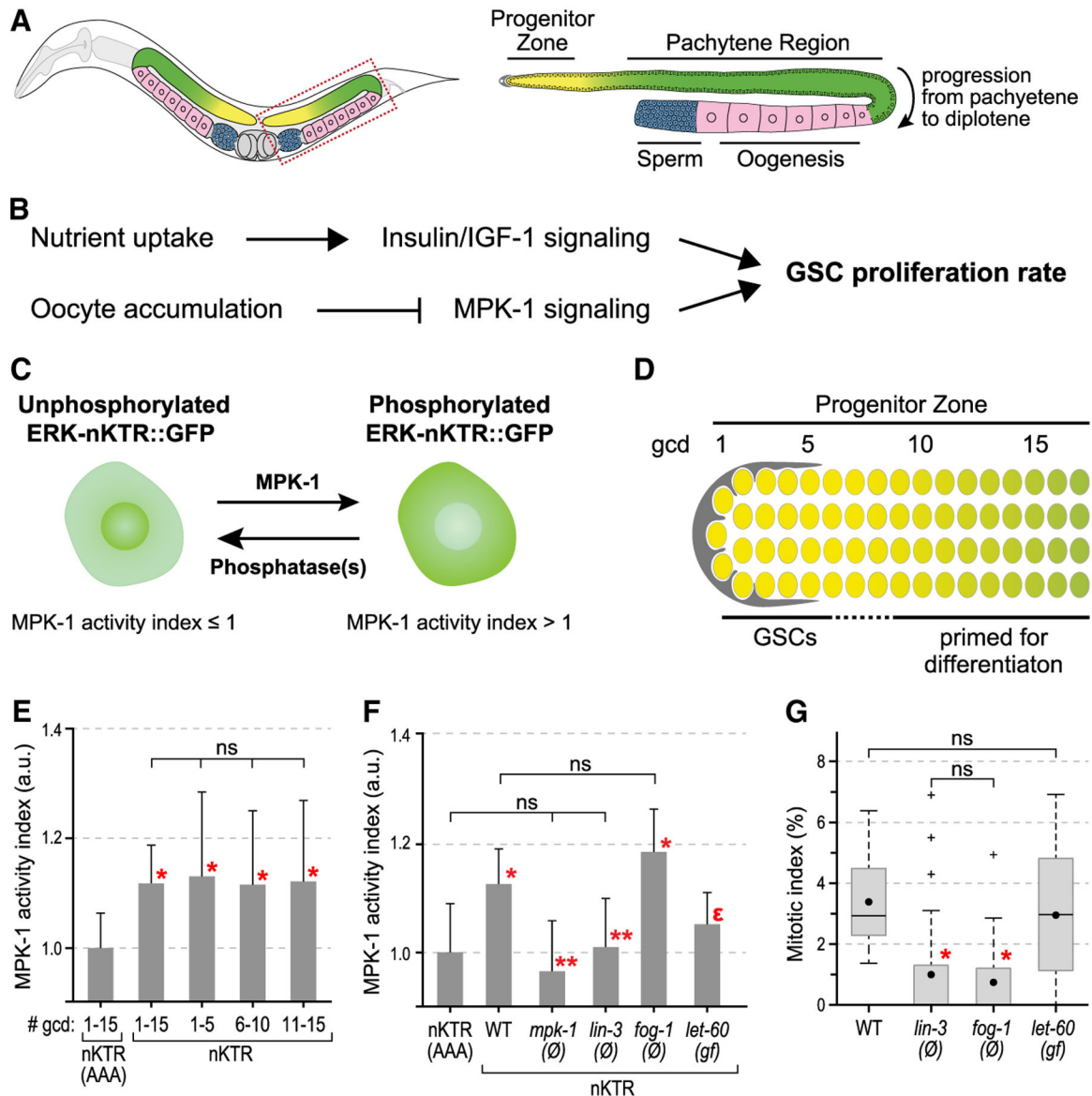


Figure 1. GSC MPK-1 activity does not correspond with GSC proliferation

(A) Left, schematic of an adult *C. elegans* hermaphrodite with posterior gonadal arm boxed.

Right, gonadal arm labeled with regions relevant to this work.

(B) GSC proliferation rate is regulated by both insulin/IGF-1 signaling and MPK-1 signaling, which act in parallel with additive effects (Narbonne et al., 2017).

(C) Schematic of *in vivo* assay for MPK-1 activity. Sensor GFP is present in the nucleus when MPK-1 activity is absent (left) but becomes cytoplasmic upon phosphorylation by MPK-1/ERK (right). The MPK-1 index refers to the ratio of cytoplasmic to nuclear GFP, normalized to the ERK-nKTR(AAA) baseline control. An index >1 indicates MPK-1 kinase activity.

(D) Proliferating germ cells in the PZ include a pool of GSCs within the niche (gray) and GSC daughters that have launched the differentiation program but not yet begun overt

differentiation. Numbers mark positions along the germline axis in germ cell diameters (gcd) from the distal end.

(E) MPK-1 activity is significant and similar across the PZ. Sample sizes are 25 animals each for nKTR and nKTR(AAA), scoring five PZ cells per animal (see Method details).

(F) MPK-1 activity is lost from the PZ in *mpk-1(ø)*, *lin-3(ø)*, and *let-60(gf)* but not *fog-1(ø)* mutants. For simplicity, nKTR(AAA) data are shown only for WT (see Figure S1 for raw ratios).

(E and F) Error bars, standard deviation. Red asterisk, statistical significance of ERK-nKTR compared with baseline ERK-nKTR(AAA) control ($p < 0.01$), determined by ANOVA followed by Tukey; ns, not significant; double asterisks, statistical significance versus the WT nKTR; e, not different from both nKTR(AAA) and nKTR controls. Sample sizes, for each (nKTR(AAA); nKTR) pair, are WT (25, 25), *mpk-1(ø)* (10, 10), *lin-3(ø)* (7, 10), *fog-1(ø)* (11, 12), *let-60 gf* (10, 10), scoring five PZ cells per animal.

(G) Boxplots of MIs in WT and mutant PZs. Dots mark averages. Red asterisk, statistical significance compared with WT ($p < 0.01$, Kruskal-Wallis followed by Dunn). Sample sizes (left to right), 14, 39, 17, 19.

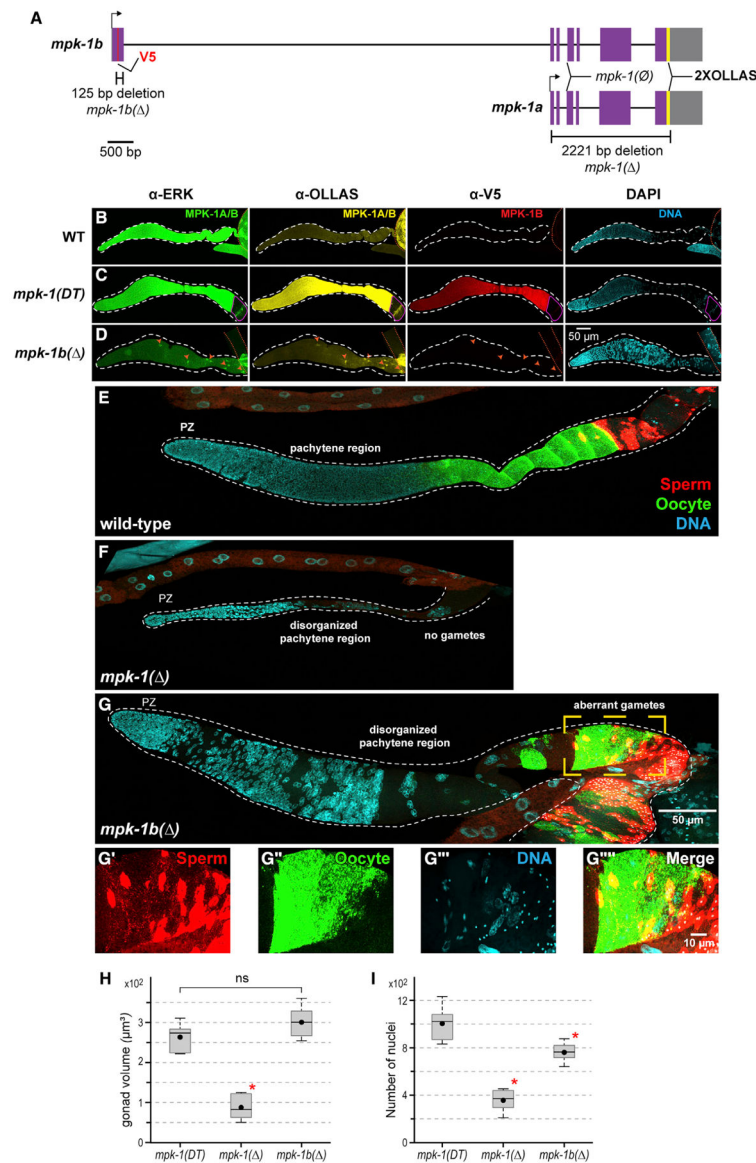


Figure 2. MPK-1B is germline-specific and promotes germline differentiation

(A) The two *mpk-1* isoforms. Purple boxes, coding exons; gray boxes, UTRs; lines connecting exons, introns; red line, V5 tag; yellow line, 2xOLLAS tags. Dual tagged *mpk-1(DT)* harbors a V5 tag in the *mpk-1b* specific exon that marks MPK-1B protein specifically, and C-terminal 2xOLLAS tags that mark both MPK-1A and B proteins. The *mpk-1b(Δ)* deletion removes most of the *mpk-1* specific exon and shifts the reading frame to eliminate MPK-1B. The *mpk-1(Δ)* deletion removes most of the shared exons and introns to eliminate MPK-1A and B (see Method details). The *mpk-1(gal17)* is considered a null (Lee et al., 2007b) and shown here as *mpk-1(∅)*.

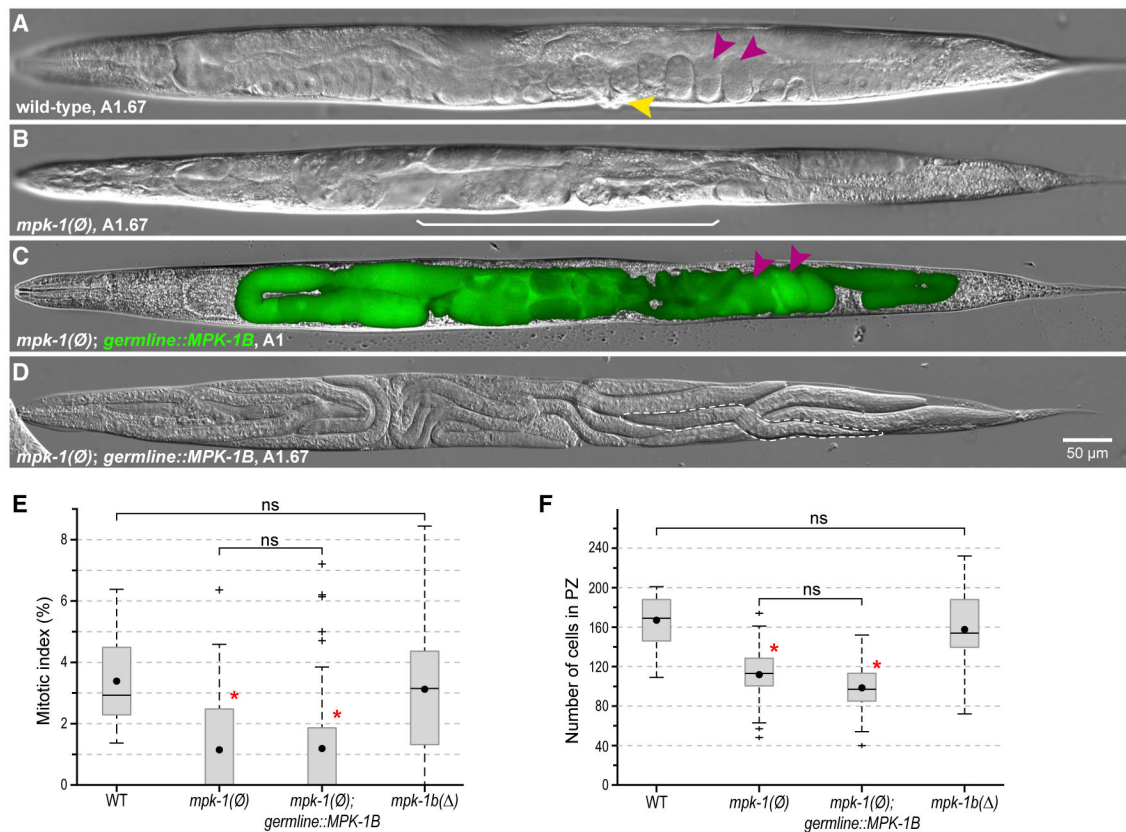
(B–G) Representative maximal projections of dissected and stained adult gonads.

(B–D) Acquisition parameters were optimized for the PZ region (see Figures S3E–S3G for quantification). When a stain does not distinguish between MPK-1A and MPK-1B, it is noted as MPK-1A/B. Anti-OLLAS staining, yellow; anti-V5 staining, red; anti-ERK

staining, green; DAPI staining, cyan. White dashed line, boundaries of germline tissue; orange dashed line, boundaries of somatic tissue. Orange arrowheads, gonadal sheath nuclei. Pink outline, zygote.

(E–G) Sperm and oocytes were stained with sp56 and RME-2 antibodies, respectively. Dashed yellow box, region magnified in D'–D'''''. (D'–D''''') Sperm and oocyte markers shown individually and merged.

(H and I) Boxplots of gonad volume and germ cell number for *mpk-1(DT)*, *mpk-1()*, and *mpk-1b()*. Gonad volume was calculated using Imaris (see Method details). Germ cells were counted manually using FIJI. Dots mark averages. Sample sizes (left to right), 10, 6, 7. Red asterisk, statistical significance versus all other samples ($p < 0.01$, ANOVA followed by Tukey); ns, not significant.



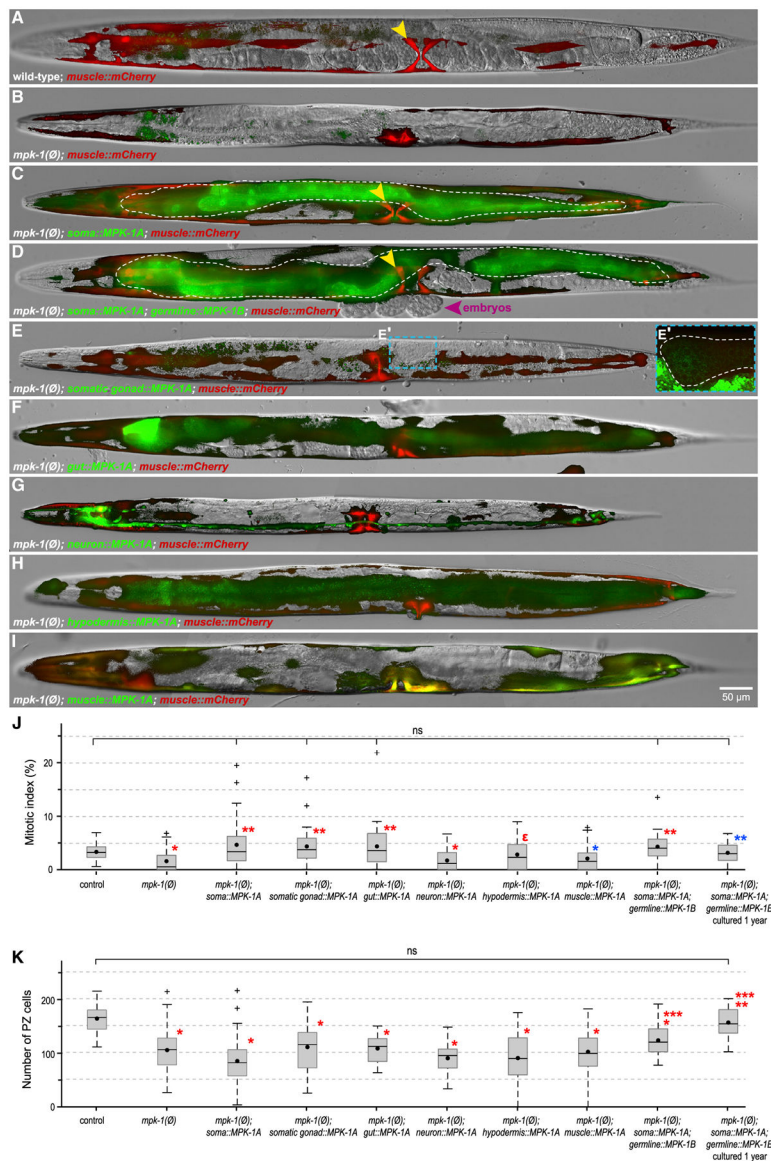


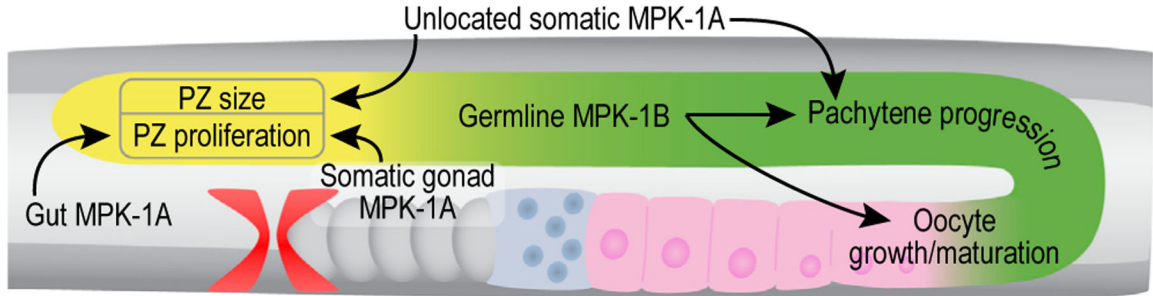
Figure 4. Somatic MPK-1A promotes GSC proliferation non-autonomously
 (A–I) Representative DIC images of A1 hermaphrodites of indicated genotypes (full genotypes in Table S4), overlaid with fluorescence signals from GFP::MPK-1A and muscle::mCherry. All animals carry *Pmyo-3::mCherry* as an extrachromosomal array marker and also to assess vulva-muscle specification (yellow arrowheads mark properly specified vulva muscles). Anterior, left. Images were not all captured with the same settings because GFP::MPK-1A levels varied from promoter to promoter, and the aim was to illustrate specificity and expression pattern. Dashed lines, gut expression in (C) and (D); somatic gonad expression in (E') (visible in larvae but barely detectable in adults; Tenen and Greenwald, 2019). Notes: For unknown reasons, animals in (D) were hypersensitive to tetramisole and laid embryos (pink arrowhead) upon paralysis. Also in those animals, GFP::MPK-1B (in the germline) was unusually low (compare with Figure 3C), likely because of co-suppression [Dernburg et al., 2000]).

(J and K) Boxplots of the PZ MI (J) and of PZ cell number (K) in A1 hermaphrodites. Dots mark averages. For each genotype, data from two to three independent lines were pooled, except for the control, where only one line was analyzed.

(J) Sample sizes (for each genotype, left to right), 24, 39, 40, 34, 31, 39, 25, 42, 27, and 21. Single asterisk, statistical significance versus control; double asterisks, versus *mpk-1(∅)*; ϵ , not different from both control and *mpk-1(∅)* (red, $p < 0.01$; blue, $p < 0.05$, Kruskal-Wallis followed by Dunn).

(K) Sample sizes, as in (J), except for *hypodermis::MPK-1A* and *muscle::MPK-1A*, which each had a sample with no PZ. Asterisks, as in (J), except using ANOVA, followed by Tukey; triple asterisks, statistical significance versus *mpk-1(∅)*; *soma::MPK-1A*.

A Germline MPK-1 functions



B Somatic MPK-1 functions

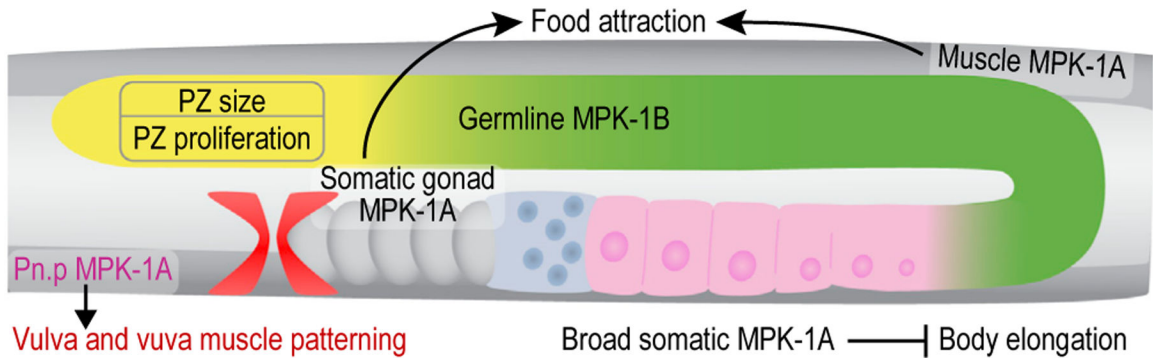


Figure 5. Models for cell autonomous and non-autonomous MPK-1 functions

(A) MPK-1 affects the germline both autonomously and non-autonomously. Germline MPK-1B autonomously promotes meiotic progression and gametogenesis. Somatic MPK-1A, on the other hand, non-autonomously ensures proper PZ size and proliferation and some, albeit abnormal, meiotic progression and gametogenesis. MPK-1A non-autonomously promotes GSC proliferation from the gut or somatic gonad, but its site of action for meiotic progression and gametogenesis remains unknown.

(B) MPK-1 activity has multiple somatic functions. Somatic MPK-1A is thought to act autonomously in the vulva (Lackner et al., 1994). It further promotes food attraction non-autonomously from the somatic gonad and muscle and can regulate body length from any somatic tissue except the gut.

(A and B) Arrows represent stimulation, and bars represent repression. Gut, light gray; germline PZ, yellow; differentiated germline, green; vulva muscles, red; body wall muscles, dark gray.

KEY RESOURCES TABLE

REAGENT or RESOURCE	SOURCE	IDENTIFIER
Antibodies		
Mouse anti-SP56	Susan Strome (University of California Santa Cruz)	N/A
Rabbit anti-RME-2	Barth Grant (Columbia)	N/A
A647-conjugated donkey anti-mouse	Invitrogen	Cat# A32787; RRID:AB_2762830
A555-conjugated goat anti-rabbit	Invitrogen	Cat# A32732; RRID:AB_2633281
Rabbit anti-ERK	Santa Cruz Biotechnologies	SCc94
Mouse anti-V5	Bio-Rad	Cat# MCA1360; RRID:AB_322378
Rat anti-OLLAS	Novis	Cat# NBP1-06713; RRID:AB_1625979
A555-conjugated donkey anti-mouse	Invitrogen	Cat# A32773; RRID:AB_2762848
A647-conjugated donkey anti-rat	Jackson ImmunoResearch	Cat# 712-605-153; RRID:AB_2340694
A488-conjugated goat anti-rabbit	Invitrogen	Cat# A32731; RRID:AB_2633280
Mouse monoclonal anti-pH3	Cell Signaling	Cat# 9706; RRID:AB_331748
Rabbit polyclonal anti-HIM-3	Monique Zetka (McGill)	N/A
A488-conjugated goat anti-mouse	Invitrogen	Cat# A-11029; RRID:AB_138404
A546-conjugated goat anti-rabbit	Invitrogen	Cat# A-11035; RRID:AB_143051
Experimental models: Organisms/strains		
<i>C. elegans</i> strains	See Table S4	N/A
Oligonucleotides		
Oligonucleotides	See Tables S5 and S6	N/A
Software and algorithms		
Zen	Zeiss.com	N/A
ImageJ	Imagej.nih.gov	N/A
Imaris	Imaris.oxinst.com	N/A